Eur. Phys. J. Appl. Phys. **83**, 10903 (2018)

https://doi.org/10.1051/epjap/2018180082

THE EUROPEAN PHYSICAL JOURNAL APPLIED PHYSICS

Regular Article

Nanofluid Al_2O_3–H_2O evaporation: energy and deposition patterns★

Tianying Li[1], Bin Liu[1,*], Xiaoyan Ma[2], and Rachid Bennacer[2]

[1] Key Lab of Refrigeration Technology, Tianjin Univ. of Commerce, 300134 Tianjin, PR China
[2] LMT/ENS-Cachan/CNRS/Paris-Saclay Univ., 61 av du Présdent Wilson, 94235 Cachan, France

Received: 6 March 2018 / Received in final form: 28 June 2018 / Accepted: 11 July 2018

Abstract. This study experimentally investigated the deposition patterns of Al_2O_3–H_2O nanofluid droplets with mass concentration of 0.05%, 0.2%, 1% and 3% after evaporating on transparent glass substrate with temperature of 30 °C, 40 °C, 50 °C and 60 °C, obtaining three typical kinds of patterns: the peripheral ring, the thin uniform layer with a thicker ring at the periphery and the concentric circular respectively. With the increase of concentration, the uniform pattern embedded in the peripheral ring changes into a concentric circular pattern gradually. The flow velocities corresponding to the three typical forces were solved and the results are $10^{-3} < V_{ma}/V_{rad-a} < 10^{-2}$ and $10^{-28} < V_{DLVO+}/V_{rad-a} < 10^{-5}$ (Marangoni, V_{ma}, the integral mean value of the entire radius V_{rad-a} and the velocity caused by DLVO force V_{DLDO+}). This indicated that the radial flow played a dominant role in the formation of the deposition pattern.

1 Introduction

If the insoluble particles are contained in droplets, they will form a certain deposition pattern on the surface of the substrate after evaporation. Different models can be applied in different fields, such as the coffee ring effect and the independent particle structure, which can be applied in the spray-ink printing [1] and the deposition process of DNA respectively. The potential application of sessile droplet evaporation in medicine is used for disease detection and diagnosis [2]. Brutin et al. studied the evaporation of whole blood droplets from different persons, obtaining diverse deposit pictures [3], and at the same time, the results of his study also pointed out that the mechanism of blood droplet evaporation could be used in forensic investigation [4]. Changing the internal parameters and external conditions are likely to produce a series of different deposition pattern, including the central aggregation type [5], combined structures and highly ordered organization of particles. Deegan et al. [6] found that for different experimental materials, the particles would move toward the edge, and form the cyclic deposition on the surface of substrate as long as three conditions were satisfied. The theoretical analysis and experimental study of Hu et al. [7] showed that the formation of deposition ring on the edge required not only the fixation of the contact line, but also the suppression of the Marangoni flow in the droplet.

Actually coffee ring pattern is formed due to the fixed contact line leading the particles radially outward flow in the suspension liquid [8,9]. The competition of the kinetics of evaporation and the interaction of the particles on the gas–liquid interface plays an important role in the formation of the uniform pattern [10]. Concentric ring is formed due to the fixation and movement of the triple-phase line [11–13]. Bhardwaj et al. [14] proposed a phase diagram to predict how the deposit shapes resulting from the competition of three typical flow patterns. However, they did not make systematic experimental study or theoretical analysis of the effects of different substrate temperatures and the different droplets concentrations on the sedimentary patterns.

In this study, experimental work was performed. Besides, further analysis was made by quantitatively calculating the corresponding velocities of the radial flow [15], the Marangoni effect and Derjaguin–Landau–Verwey–Overbeek (DLVO) force.

2 Experimental method

The Al_2O_3–H_2O nanofluid dispersion (Hangzhou Wanjing New Material Co. Ltd, an average diameter of 10 nm, a mass fraction of 20%) was diluted with deionized water into four different mass fractions of 0.05%, 0.2%, 1% and 3%. The nanofluids were stirred by the magnetic heating agitator (Jintan Zhongda Instrument Co. Ltd, 78-1) for one hour, and then vibrated by the ultrasonic cell disruptor (Nanjing Xianou Instrument Manufacturing Co. Ltd, XO-150) to make the particles well-dispersed. The droplets deposited on a slide glass surface whose temperature was controlled at 30 °C, 40 °C, 50 °C and 60 °C, respectively,

★ Contribution to the topical issue "Materials for Energy harvesting, conversion and storage (Icome 2017)", edited by Jean-Michel Nunzi, Rachid Bennacer, and Mohammed El Ganaoui.

* e-mail: lbtjcu@tjcu.edu.cn

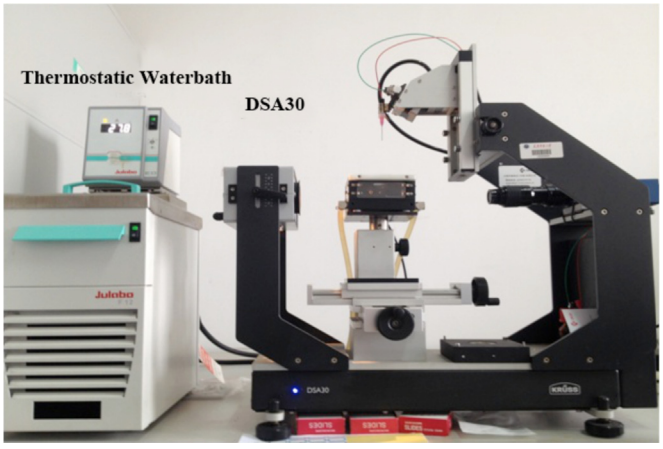

Fig. 1. The measurement equipment of the droplet in evaporation (DSA30 and Thermostatic Waterbath).

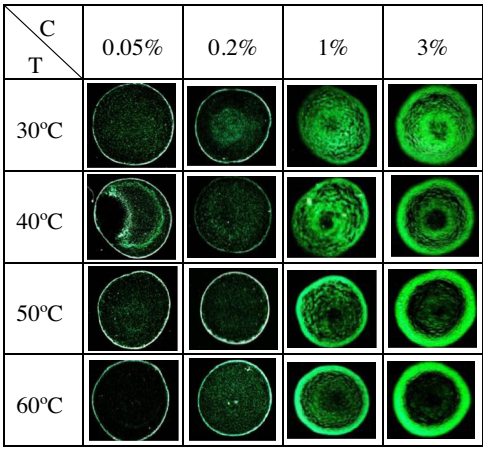

Fig. 2. The 10 times larger pictures of deposition patterns taken by the gem microscope.

with the thermostatic waterbath (Julabo, F12). The indoor temperature was $20 \pm 0.2\,^{\circ}\mathrm{C}$, and the relative humidity was $30 \pm 1\%$. The experiments with same parameters were repeated five times to ensure the reliability of the experiment.

The evaporation process of droplet was recorded by the droplet shape analyzer (KRUSS, DSA30), as shown in Figure 1, and then the evolution of contact angle and contact radius of the droplet with time were obtained by the measuring software.

After evaporation, the deposits were observed with the gem microscope (MOTIC, GM168, magnification 10–80 times) to get the whole deposit shapes.

3 Results and discussion

3.1 Experimental results

Figure 2 shows 10 times larger pictures of deposition patterns taken by the gem microscope. For the lower concentration (0.05% and 0.2%), the coffee ring effect is more obvious, but for the higher concentrations (1% and 3%), concentric rings are formed. At the same temperature, the edge of the coffee ring becomes wide with the increasing of concentration, and for a constant concentration, the deposition of nanoparticles at the edge is more and more obvious with the increasing of substrate temperature.

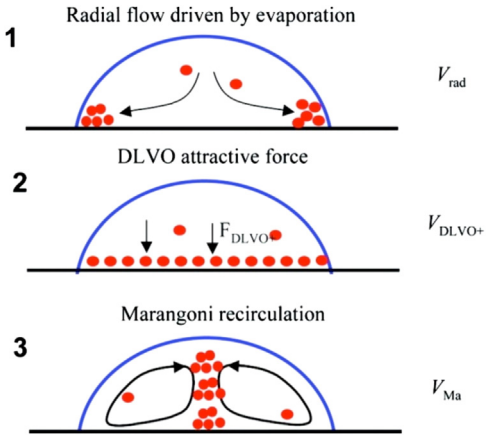

Fig. 3. Three convective mechanisms compete to form the deposit. In (1), a ring forms due to the radial flow caused by the maximum evaporation rate at the triple-phase line; in (2), a uniform deposit forms due to an attractive DLVO force between the particles and the substrate; in (3), a central bump forms due to a Marangoni recirculation loop.

Table 1. The dynamic viscosity of the nanofluid.

C/%	$\mu_{nf}/10^{-5}$ Pa·s			
	30 °C	40 °C	50 °C	60 °C
0	80.07	65.60	54.94	46.88
0.05	80.45	65.91	55.20	47.10
0.20	81.60	66.86	55.99	47.78
1	87.98	72.08	60.36	51.51

3.2 Theoretical analysis

Based on the experimental data, the magnitude of three typical flow patterns is estimated by analytical relations. The flow and deposition of the nanoparticles at the three velocities are shown in the Figure 3 [14].

The dynamic viscosities of the nanofluid are given in Table 1 according to the computational formulas [16–18].

3.2.1 The radial flow

Deegan et al. [6] found there was a good agreement between experimental results and theoretical predictions for the vertically averaged radial flow velocity, which scaled as

$$V_{rad} \sim (R-r)^{-\lambda}, r \geq \frac{1}{3}R,$$

$$\lambda = \frac{\pi - 2\theta}{2\pi - 2\theta} \quad (1)$$

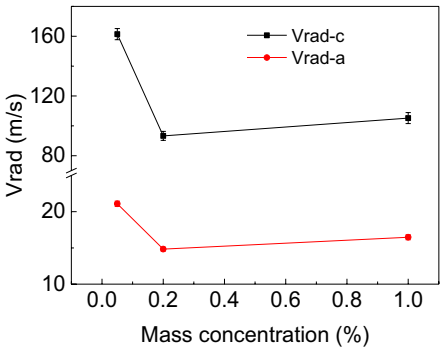

Fig. 4. The initial mean radial velocity with different concentrations at 50 °C (mean value of the entire radius V_{rad-a} and the average velocity V_{rad-c} of different positions $R-r$ of 1, 10 and 100 μm ($R>r>R/3$)).

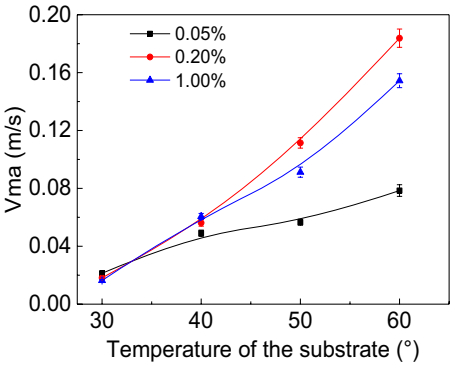

Fig. 5. The variation curve of incipient V_{ma} with temperatures and concentrations.

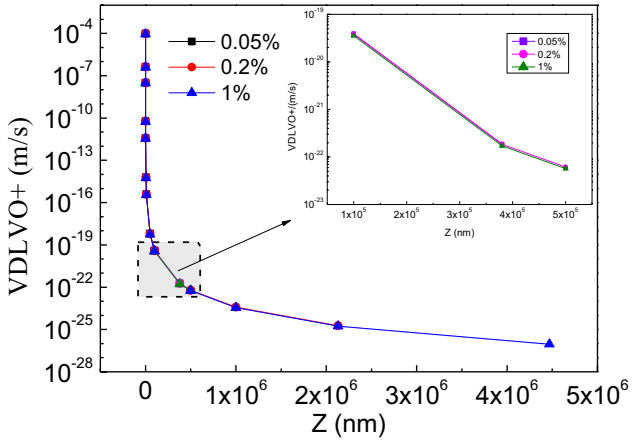

Fig. 6. The variation of the incipient V_{DLVO+} with the Z for different concentrations.

where R is the contact radius [m], r is a radial distance from the center of the drop [m], and θ is the contact angle of the droplet [rad].

Figure 4 shows the average radial velocity $V_{rad-a} > 10^1$, the average value near the contact line $V_{rad-c} > 10^2$ and diverging at the contact line. The V_{rad} increases with time and diverges at the end of the evaporation according to the analysis of Deegan et al. [6]. The expression is based on the diffusion-limited theory not considering the influence of the substrate temperature. Obviously, the evaporation process will be accelerated with the increasing of the substrate temperature, then leading to the actual speed far greater than the above values.

3.2.2 Marangoni circulation loop

An analytical expression for the typical loop velocity is provided by Hu and Larson [19] and scales as:

$$V_{ma} \sim \left(\frac{1}{32}\right)\left(\frac{\beta\varphi^2\Delta T}{\mu}\right) \tag{2}$$

In this equation (2), β is the gradient of surface tension with respect to the temperature (-0.1657×10^{-3} N/m·k), φ is the wetting angle of the drop [rad], μ is dynamic viscosity [Pa·s], and ΔT is the temperature difference between the edge and the top of the droplet [K].

From Figure 5, $10^{-2} < V_{ma} < 10^0$, as the evaporation goes on, the temperature difference between top and edge becomes smaller and smaller [20], and the contact angle also decreases with time, which result in V_{ma} gradually decreasing over time, namely Marangoni effect gradually declining.

3.2.3 Attractive DLVO force

In this study, no hydrochloric acid or sodium hydroxide is added to the Al_2O_3 nanofluids, therefore, ignoring the electrostatic force, the V_{DLVO+} [14,21,22] scales as:

$$V_{DLVO+} \sim \frac{Ad_p^2\alpha_{rtd}}{36\pi\mu Z^2(Z+d_p)^2} \tag{3}$$

where A is the Hamaker constant, $A = 2.43\times10^{-20}$ J [23], α_{rtd} is the retardation factor for the van der Waals force, taking 0.1 here [22], d_p is diameter of particles (10 nm), and Z is the distance between the particle and the substrate [m].

The incipient V_{DLVO+} varies with the Z valued in proper order from 10 nm to h the highest point of the droplet for different concentrations as shown in Figure 6. ($h = R - R\cos\theta$)

Figure 6 shows the V_{DLVO+} is almost the same for different concentrations and increases dramatically with the decrease of Z, finally $10^{-27} < V_{DLVO+} < 10^{-4}$. Besides, the higher the temperature is, the bigger the V_{DLVO+} is.

Furthermore, $10^{-28} < V_{DLVO+}/V_{rad-a} < 10^{-5}$, combined $10^{-3} < V_{ma}/V_{rad-a} < 10^{-2}$, it can be concluded that the final deposition patterns should be based on the coffee ring and probably show a thin uniform layer inside the ring under the competition of the DLVO force and the Marangoni effect, which match the experimental results.

4 Analysis of the concentric circular

For the approximate concentric circular pattern formed at the concentration of 1%, we added a set of experimental studies for the mass concentration of 3%, as shown in Figure 2.

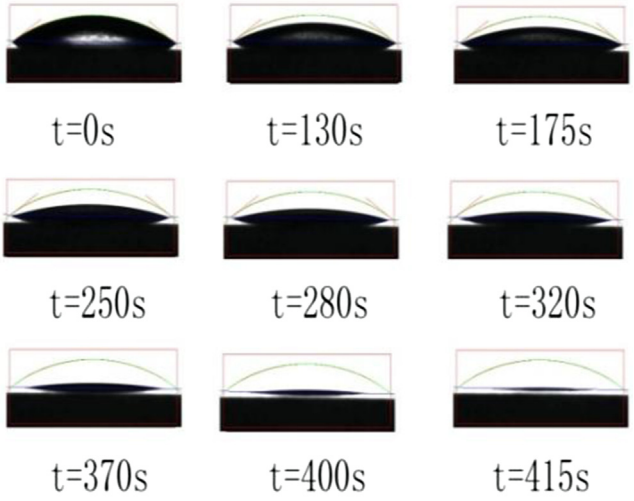

Fig. 7. Profile evolution of 1% nanofluid sessile droplet on glass substrate of 30 °C.

The droplet evaporation model in this experiment is close to the stationary contact line until the final stage decreasing rapidly and sudden change to 0 shown in Figure 7.

The above analysis indicates that the radial flow plays a dominant role in the formation of the deposition pattern. Because the majority of the particles have moved to the edge during the fixed stage of the contact line, the remaining particles will form a inner ring following the triple-phase line for the higher concentration case. Meanwhile, since the radial velocity increases rapidly, even diverges at the end of the evaporation, a hollow internal circle is formed.

With the increase of temperature and the enhance of evaporation, the radial velocity is improved continuously, and most of the particles in the approximate fixed stage has deposited in the triple-phase line reducing the quantity of particles following the movement of contact line, so the concentration of internal concentric circle peters out.

It can be seen from the above deposition patterns that the concentration of nanoparticles is also an important factor affecting the combination of nanoparticles.

5 Conclusion

Based on the above experimental and analytical results, the following conclusions can be obtained:

– The experimental deposition patterns include the peripheral ring, the thin uniform layer with a thicker ring at the periphery and the concentric circular.
– The magnitude of three typical flow patterns is estimated by analytical relations based on the experimental data, and the conclusion that the deposit patterns are based on the coffee ring coincides with the experimental results.
– The radial flow caused by the maximum evaporation rate at the triple-phase line is dominant for the formation and variation of concentric circles.

Author contribution statement

Tianying Li and Bin Liu contributed to the conception of the study. Tianying Li and Xiaoyan Ma performed the experiments. Tianying Li analyzed the data and wrote the manuscript. Bin Liu and Rachid Bennacer helped perform the analysis with constructive discussions. Rachid Bennacer and Xiaoyan Ma checked the expression and the grammar of English.

The authors gratefully acknowledge financial support from the Foundation of Tianjin Education Committee (170018).

References

1. L. Zhang et al., Adv. Mater. **24**, 436 (2012)
2. K. Sefiane, J. Bionic. Eng. **7**, S82 (2010)
3. D. Brutin et al., Fluid Mech. **667**, 85 (2011)
4. D. Brutin, B. Sobac, C. Nicloux, J. Heat Transf. **134**, 061101 (2012)
5. C.T. Chen, F.G. Tseng, C.C. Chieng, Sens. Actuators A Phys. **130** (2006)
6. R.D. Deegan et al., Phys. Rev. E **62**, 756 (2000)
7. H. Hu, R.G. Larson, Phys. Chem. B **110**, 7090 (2006)
8. R.D. Deegan, Phys. Rev. E **61**, 475 (2000)
9. K. Sefiane, Adv. Colloid Interface Sci. **206**, 372 (2014)
10. T.P. Bigioni et al., Nat. Mater. **5**, 265 (2006)
11. J.R. Moffat, K. Sefiane, M.E. Shanahan, Phys. Chem. B **113**, 8860 (2009)
12. D. Orejon, K. Sefiane, M.E. Shanahan, Langmuir **27**, 34 (2011)
13. E. Adachi, A.S. Dimitrov, K. Nagayama, Langmuir **11**, 1057 (1995)
14. R. Bhardwaj et al., Langmuir **26**, 7833 (2010)
15. J.M. Stauber, S.K. Wilson, B.R. Duffy, Langmuir **31**, 3653 (2015)
16. Y. Xuan, Q. Li, *Theory and Application of Nanofluid Energy Transfer* (Science Press, Beijing, 2010)
17. H.C. Brinkman, J. Chem. Phys. **20**, 571 (1952)
18. A. Einstein, Ann. Phys. **324**, 289 (1906)
19. H. Hu, R.G. Larson, Langmuir **21**, 3972 (2005)
20. T. Li, B. Liu, Q. Li, in *Proceedings of the Academic Conference of China Engineering* (Thermal Physics Society, Suzhou, 2017)
21. M. Kobayashi, H. Nanaumi, Y. Muto, Colloids Surf. A **347**, 2 (2009)
22. C. Tien, *Granular Filtration of Aerosols and Hydrosols* (Butterworths, Boston, 1989)
23. P.C. Hiemenz, R. Rajagopalan, *Principles of Colloid and Surface Chemistry*, 3rd edn. (Marcel Dekker, New York, 1997)

Cite this article as: Tianying Li, Bin Liu, Xiaoyan Ma, Rachid Bennacer, Nanofluid Al_2O_3–H_2O evaporation: energy and deposition patterns, Eur. Phys. J. Appl. Phys. **83**, 10903 (2018)